


# First Observation of Cross-Beam Energy Transfer Mitigation for Direct-Drive Inertial Confinement Fusion Implosions Using Wavelength Detuning at the National Ignition Facility

J. A. Marozas,<sup>1,\*</sup> M. Hohenberger,<sup>1</sup> M. J. Rosenberg,<sup>1</sup> D. Turnbull,<sup>1</sup> T. J. B. Collins,<sup>1</sup> P. B. Radha,<sup>1</sup> P. W. McKenty,<sup>1</sup> J. D. Zuegel,<sup>1</sup> F. J. Marshall,<sup>1</sup> S. P. Regan,<sup>1</sup> T. C. Sangster,<sup>1</sup> W. Seka,<sup>1</sup> E. M. Campbell,<sup>1</sup> V. N. Goncharov,<sup>1</sup> M. W. Bowers,<sup>2</sup> J.-M. G. Di Nicola,<sup>2</sup> G. Erbert,<sup>2</sup> B. J. MacGowan,<sup>2</sup> L. J. Pelz,<sup>2</sup> and S. T. Yang<sup>2</sup>

<sup>1</sup>Laboratory for Laser Energetics, University of Rochester, 250 East River Road, Rochester, New York 14623-1299, USA

<sup>2</sup>Lawrence Livermore National Laboratory, 7000 East Avenue, Livermore, California 94550-9698, USA

 (Received 3 May 2017; published 22 February 2018)

Cross-beam energy transfer (CBET) results from two-beam energy exchange via seeded stimulated Brillouin scattering, which detrimentally reduces ablation pressure and implosion velocity in direct-drive inertial confinement fusion. Mitigating CBET is demonstrated for the first time in inertial-confinement implosions at the National Ignition Facility by detuning the laser-source wavelengths ( $\pm 2.3 \text{ \AA}$  UV) of the interacting beams. We show that, in polar direct-drive, wavelength detuning increases the equatorial region velocity experimentally by 16% and alters the in-flight shell morphology. These experimental observations are consistent with design predictions of radiation-hydrodynamic simulations that indicate a 10% increase in the average ablation pressure.

DOI: 10.1103/PhysRevLett.120.085001

In direct-drive inertial confinement fusion (ICF), laser beams irradiate a plastic coated shell of frozen deuterium-tritium (DT) and ablatively drive an implosion. The ultimate goal of ICF is ignition and energy gain; the minimum shell kinetic energy required for ignition (defined as when the energy from DT fusion reactions exceed the laser energy incident on the target) is given by  $E_{\min} \sim \alpha^{1.88} P_{\text{abl}}^{-0.77} v_{\text{imp}}^{-5.89}$  [1], where the three parameters of the implosion,  $\alpha$ ,  $v_{\text{imp}}$ , and  $P_{\text{abl}}$  [adiabat (the ratio of the fuel pressure to the Fermi-degenerate pressure at peak implosion velocity), implosion velocity, and ablation pressure, respectively] are determined primarily by the deposition of the laser energy into the coronal plasma of the target and heat conduction to the ablation surface. Cross-beam energy transfer (CBET) [2] has been identified in direct-drive experiments on the OMEGA [3] and National Ignition Facility (NIF) [4] lasers to reduce absorption, ablation pressure, and implosion velocity.

The role of CBET in direct drive was identified in early research [5,6], but was only recently identified as the leading cause of decreased energy coupling. When attempts were made to match multiple calculated observables (shell morphology, trajectory, scattered-light spectra and distribution, and shock timing) with experiments, the critical role of CBET became apparent [7,8], which lowers laser absorption by 20%–30%. Good agreement with the multiple experimental observables was obtained [7,8] when both the CBET and nonlocal electron transport [9] models were included in one-dimensional LILAC [10] and two-dimensional DRACO [11] simulations. Historically, the role

of CBET [5,6] was masked by using a flux-limited electron transport model matching laser absorption.

CBET laser-plasma interaction results from two-beam energy exchange via stimulated Brillouin scattering (SBS) [2], which reduces absorbed light and consequently reduces ablation pressure and implosion velocity. The dominant CBET loss mechanism in direct drive occurs when rays counterpropagate (backscatter mode), increasing scattered light, as illustrated in Fig. 1(a). For the ignition-relevant overlapped beam intensities of  $\sim 8 \times 10^{14} \text{ W/cm}^2$  for these NIF experiments, CBET is calculated to reduce laser absorption by 22%, the average implosion speed by  $\sim 9\%$ , and the average ablation pressure by 35%. These drive-related results are consistent with other ongoing OMEGA- [7] and NIF-scale [8] experiments. Reducing

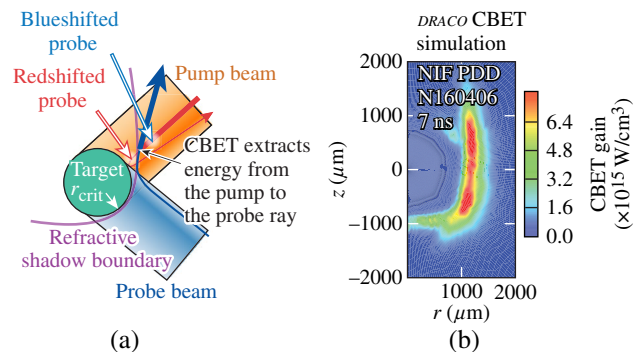


FIG. 1. (a) The effect of CBET in PDD predominantly affects the equatorial region; (b) successful CBET mitigation benefits the same region.

the target mass compensates for CBET losses, but the thinner shells become compromised as a result of instability growth [12]. As shown by the above equation for  $E_{\min}$ , efficient laser energy coupling and hydrodynamic stability are essential aspects of direct-drive ICF, making CBET mitigation vital. Mitigation strategies of the deleterious CBET effects invoke combinations of spatial, temporal, and wavelength domains. Wavelength detuning, the focus of this Letter, works by altering the resonance condition between interacting beams [2]. Wavelength detuning was first examined for indirect drive [13] and subsequently for direct drive, but was prematurely dismissed as a viable option [14].

The first direct-drive experiments have been designed for the NIF to study the efficacy of wavelength-detuning CBET mitigation. The target designed for these wavelength-detuning shots on the NIF was adapted from existing 600-kJ designs [8], where the trajectories and the shape of the imploding shell and scattered light were well described by the CBET model in DRACO. The basic target design is shown in the inset of Fig. 2, where the laser beam powers (shown in red) produce a peak overlapped intensity of  $\sim 8 \times 10^{14}$  W/cm<sup>2</sup> at the initial target radius.

The indirect-drive NIF beam geometry distributes 192 beam ports [grouped into 48 quads, shown as circles in Fig. 3(a)] toward the poles of the NIF target chamber, forming cones of quads with a common polar angle [15]. Repointing higher-intensity beams from lower latitudes toward the equator partially compensates for the NIF port geometry and higher incident angles when illuminating direct-drive targets. In this modified configuration, referred to as polar direct drive (PDD) [16,17], CBET predictably dominates in the equatorial region where most of the cross-beam interactions occur, as shown in Fig. 1(b). As a result, PDD implosions tend to become oblate because CBET reduces the laser drive preferentially in the equatorial region. With this motivation, a basic wavelength-detuning strategy exploits the PDD configuration, where each hemisphere has a different wavelength or color. However, the

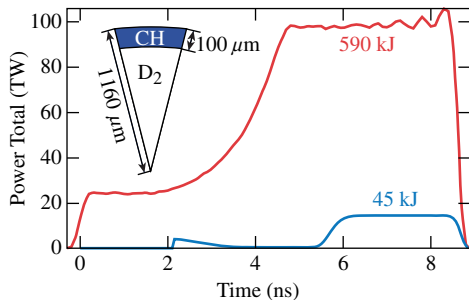


FIG. 2. The NIF PDD target design for wavelength detuning with cone swapping to induce a wavelength difference across the equator. (Inset) The warm plastic (CH), 1160- $\mu\text{m}$ -radius, 100- $\mu\text{m}$ -thick shell with a 20-atm  $\text{D}_2$  gas fill; (red) the total 590-kJ design pulse; (blue) the 45-kJ backlighter pulse.

nominal symmetric wavelength mapping [see Fig. 3(a)] developed for indirect-drive targets precludes achieving hemispheric wavelength detuning using typical PDD repointing configurations [17].

The NIF fiber front end [15] supports three separate initial colors or wavelength shifts  $\Delta\lambda_0 = \{\lambda_1, \lambda_2, \lambda_3\}$  detuned from a central wavelength  $\lambda_0 \sim 351$  nm. Currently, the three-color  $\{\lambda_1, \lambda_2, \lambda_3\}$  mapping onto the NIF indirect-drive ports is symmetric about the equator [see Fig. 3(a)]. To induce a wavelength difference about the equatorial region, a dramatic repointing (referred to as “cone swapping”) is required in either the northern or southern hemisphere [see Fig. 1(b) for the southern case]. For cone swapping, in one hemisphere the higher-latitude ports (“inner cones”  $\{\lambda_1, \lambda_2\}$ ) are repointed to the equator and the lower-latitude ports (“outer cones”  $\{\lambda_3\}$ ) are repointed to the mid and high latitudes. For the wavelength-detuning experiments described here, two different colors were specified, such that  $\lambda_1 = \lambda_2 \neq \lambda_3$ , although future enhanced experiments with three colors are planned. The current NIF configuration, while not optimal, is capable of achieving a modest wavelength-detuning level,  $\Delta\lambda_0 = \{2.3, 2.3, -2.3\}$  Å UV, which is adequate for these proof-of-principle experiments. Cone swapping plus wavelength detuning induces the desired partial hemispheric wavelength difference between beams crossing the equatorial region.

The far-field spot envelope [induced from distributed phase plates (DPPs) [18] and small-divergence smoothing] quad mapping is given by the current indirect-drive configuration on the NIF: the inner cones ( $\lambda_1, \lambda_2$ ; red and green circles) use a wide elliptical spot shape not well suited for the equatorial region, while the outer cones ( $\lambda_3$ ; blue circles) use a narrow elliptical spot shape. The values of the beam energy and repointing were additionally adjusted in the cone-swapping hemisphere to compensate for the swapped spot shapes and the higher incident angles using established PDD design principles [17]. The cone-swapping repointing scheme and the fixed DPP quad

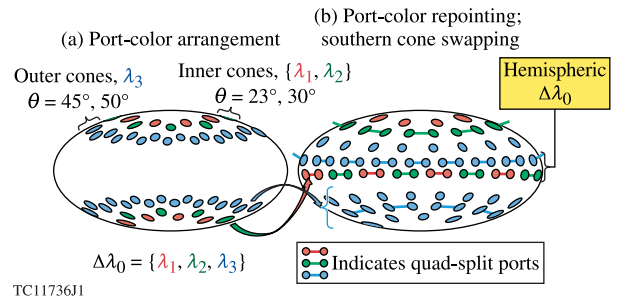


FIG. 3. NIF quad-port hammer projections for the wavelength-detuning CBET mitigation scheme. (a) Indirect-drive mapping where the colored symbols indicate relative wavelength; (b) PDD repoint mapping that achieves hemispheric detuning, typical northern hemisphere repointing, and southern hemisphere cone swapping.

mapping result in nonoptimal implosion symmetry; see Fig. 3(b). For this reason, fusion yield and areal density are not metrics for these experiments, which concentrate instead on observables directly related to laser energy absorption: implosion trajectory, shell morphology, and scattered light. Future reconfigurations (optimal DPPs for PDD [17,18], flexible color mapping, and larger wavelength separation) can relieve these constraints and simulations predict improved overall fusion performance.

In direct drive, many overlapping beams interact with each other in a complicated tangle of intensity, directions, and wavelengths depending on the beam-port configuration surrounding the imploding target. In addition, each beam strongly refracts and chirps in the expanding, evolving plasma atmosphere during propagation and then scatters in a wide spread of exiting paths. The DRACO CBET package (Adaawam) is an integral part of the 3D ray-trace package (Mazinisin) [17], which models each beam as a set of adaptively chosen rays to minimize noise. An extension to the plane-wave CBET model [2] adapts the steady-state fluid model to 3D interacting rays in Adaawam by generalizing the wave-vector phase-matching condition. The CBET model [2] includes relevant SBS physics and results in gain or loss for a probe-ray interacting with the total pump angular spectrum. Adaawam calculates the CBET interaction self-consistently in conjunction with the hydrodynamic evolution of the ICF target (via a split-step technique) and captures the necessary coupled interaction of the dynamic electron density profile, temperature, and plasma-flow velocity that dictates the behavior of CBET, and vice versa, since CBET and the hydrodynamics are strongly coupled. Adaawam uses advanced iterative feedback control to stabilize the CBET tightly coupled many-beam interactions while maintaining energy conservation. This model has been compared to many observables across a range of implosions on OMEGA [19] and the NIF [7]. An experimentally determined CBET-gain multiplier of 1.5 (from unrelated OMEGA shots [19]) was applied to all pre- and postshot simulations without attempting to fit the NIF shots having similar intensity, but different scale lengths and pulses.

Maximal CBET occurs in the rapidly expanding coronal plasma where two interacting rays satisfy the ion-acoustic-wave-matching conditions [2,13,14] that account for propagation direction, wavelength, and fluid flow; e.g., a CBET resonance occurs at the Mach 1 surface for directly opposed rays of equal wavelength. The instantaneous ray wavelength is given by its initial value and the temporal derivative of the electron density (an extension of the common Doppler shift [20]), which dynamically alters the instantaneous refractive index in space, and thereby the wavelength, and is independent of ray direction. Consequently, the CBET resonance features are altered as the coronal plasma evolves, which directly maps onto a chirped scattered-light measurement that can be employed to help analyze the implosions and laser-plasma interaction

physics. A future publication will address the complete set of measurements and modeling.

Wavelength detuning between crossing beams responds differently in indirect- versus direct-drive ICF implosions, depending on the dominant CBET mode. In indirect drive, the sign of small wavelength detuning ( $< 2 \text{ \AA}$  UV) is used to control the direction of energy transfer between interacting beams by leveraging the CBET resonance for the forward-scatter mode [13]. (While this mode occurs in direct drive, it does not increase scattered-light loss.) In contrast, an outbound ray in the dominant backscatter mode in direct drive experiences CBET gain regardless of the wavelength-difference sign or magnitude (for nominal levels) because the ion-acoustic wave's contribution dominates the CBET resonance function. Under atypical conditions, the outbound ray may experience a loss resonance but insignificantly impacts scattered light because the outbound rays typically transport little energy. The ensemble CBET exchange is best described as an interaction volume (a weighted volume that determines the interaction strength, which depends on path length, intensity, wavelength, electron density, coronal temperature, fluid velocity, etc.) because any high-gain region is equally matched by loss, and significant CBET occurs only when the ensemble interaction volume is large. For example, there might be high intensity near a turning point over insignificant path lengths that form an ineffective and small interaction volume with minimal resulting CBET.

The resonant CBET gain region of the outbound rays in the backscatter mode never completely disappears, but rather shifts into a smaller interaction volume because the relative instantaneous wavelength difference changes the ion-acoustic-wave-matching conditions of the interacting rays. The resonance region bifurcates and shifts both farther out in the corona (where the outbound rays have lower intensity and experience higher expanding fluid velocity and lower electron density) and closer inside the corona (where the interaction becomes shielded by the refractive shadow-boundary surface and/or outbound rays that have negligible intensity) [see Fig. 1(a)]. A sufficiently large wavelength separation (detuning) significantly reduces CBET exchange for direct drive by decreasing the interaction volume. In contrast, an insufficient wavelength separation can lead to deposition and shell distortion via the forward-scatter mode. The efficacy of wavelength-detuning CBET mitigation diminishes as the plasma expands and the target implodes, which causes the CBET resonance regions to gradually drift into larger interaction volumes during the drive pulse. Larger wavelength-detuning values delay the onset of diminished mitigation. Simulations predict that wavelength-detuning CBET mitigation is effective for both symmetric direct drive (OMEGA) and PDD since the same mechanisms occur in both configurations, although the positive impact is more pronounced for PDD.



With this motivation, for the first time in direct-drive ICF, wavelength-detuning CBET mitigation was demonstrated and shown to improve energy coupling. The NIF PDD wavelength-detuning CBET mitigation campaign shots were performed in three pairs; each pair consisted of one implosion backlit with  $\sim 6.7$ -keV x rays produced from a planar Fe foil target energized by two quads of NIF beams with 45 kJ (see the blue curve in Fig. 2) of UV laser energy per beam with an equatorial view of the compressing shell and a second implosion for soft x-ray self-emission images of the compressing target from equatorial and polar views. Additional diagnostics measured both hard x rays produced by energetic electrons and scattered light arising from the stimulated Raman and possible two-plasmon-decay instabilities. The inferred levels contain at most only a few percent of the incident energy and do not affect the analysis of the laser-target coupling and CBET [7]. The first pair of control experiments (shots N160405 and N160406) with the same wavelength for all the beams (zero detuning) was performed to establish the baseline experimental observables. Next, two pairs of experiments with a detuning mapping of  $\Delta\lambda_0 = \{2.3, 2.3, -2.3\}$  Å UV were performed to evaluate the efficacy of wavelength-detuning CBET mitigation. The zero- and first-detuning shots (N160821-001 and N160821-002) employed southern-hemisphere cone swapping, as illustrated in Fig. 3(b). The second-detuning shots (N170102 and N170103) employed northern-hemisphere cone swapping, primarily to effectively image the self-emission from the opposite pole and to observe the expected image inversion. The repointing (accounting for mirror-image cone swapping) and pulse shapes were nominally identical for all shots, where the only intended difference was the wavelength configuration.

The simulated and measured backlit gated x-ray radiographs are analyzed to show shell morphology evolution as well as in-flight shell trajectory, which are used to infer energy coupling. The gated images (gate time  $\sim 100$  ps) shown in Fig. 4 compare the shell morphology for the three backlit shots. The experimental framing-camera images are a composite of several images close in time for this slowly moving target that were cross correlated and adjusted for magnification to enhance the signal-to-noise ratio; the measurements used a  $30$ - $\mu\text{m}$  pinhole. The simulated images are postprocessed with the x-ray imaging code Spect3D [21] with matching pinholes and gates. The first two rows are radiographs of matched postshot simulations and experimental results for the baseline zero- and wavelength-detuning shots with southern-hemisphere cone swapping. The last row shows radiographs for detuning shots with northern-hemisphere cone swapping. All the backlit radiograph data show remarkable agreement between simulation and experiment, especially the expected trend for the detuning shots. A mere  $\sim 2\%$ – $3\%$  additional laser energy is absorbed with detuning, but since this energy is localized

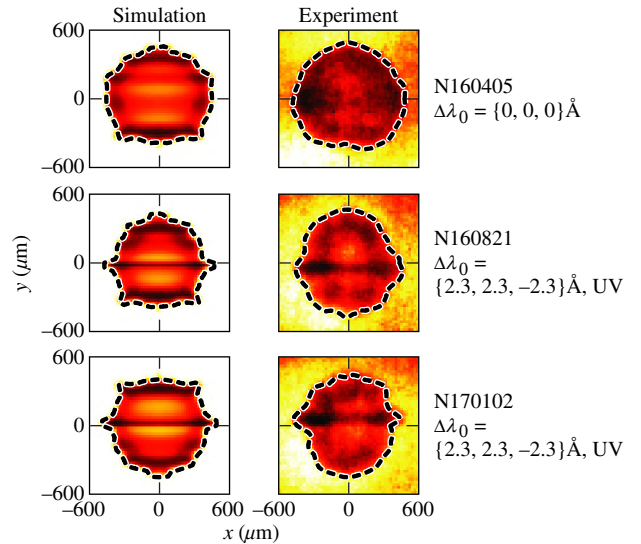


FIG. 4. Comparison of backlit radiographs from postshot DRACO simulations and NIF experimental results near the end of the laser pulse at  $t = 8.5$  ns. The dashed lines indicate the outer shell surface extracted from each image defined by the steepest gradient in the inward radial direction.

to the equatorial coronal volume fraction ( $\sim 25\%$ ), and the deposition is redistributed to increase hydrodynamic efficiency, the result is dramatic as observed with the gated x-ray radiographs.

Most notable was the design prediction and measurement of the equatorial mass accumulation near the equator with active wavelength detuning (bottom two rows in Fig. 4). As predicted, the mass accumulation flipped orientation when cone swapping was applied to the opposite hemisphere. The wavelength-detuning design attempted to minimize the  $\ell = 2$  Legendre mode, while accounting for the spot shapes, pointing, and energies in conjunction with the expected increased drive in the equatorial region caused by CBET mitigation. The equatorial mass accumulation is a common feature in PDD designs (and not directly related to CBET mitigation), which is caused by lateral mass flow toward the equator (from primarily oblique incidence) when sufficient equatorial drive is available (e.g., from CBET mitigation) and when using nonoptimal spot shapes while achieving a small  $\ell = 2$ .

The shell trajectory is inferred from the simulated and experimental backlit radiographs by first extracting the outer steepest gradient surface or radii [see Figs. 4 and 5 (inset)]. The majority of the CBET gain occurs in the equatorial region [Fig. 1(b)] and, consequently, the region expected to benefit from wavelength detuning. Both the surface-area weighted average of the whole extracted surface and a range restricted to the equatorial region (shown here) demonstrate the benefit. When the extracted shell surface is restricted to the equatorial region ( $\pm 30^\circ$  region about the equator) and plotted as a function of time (see Fig. 5), the inferred implosion speed increases as a

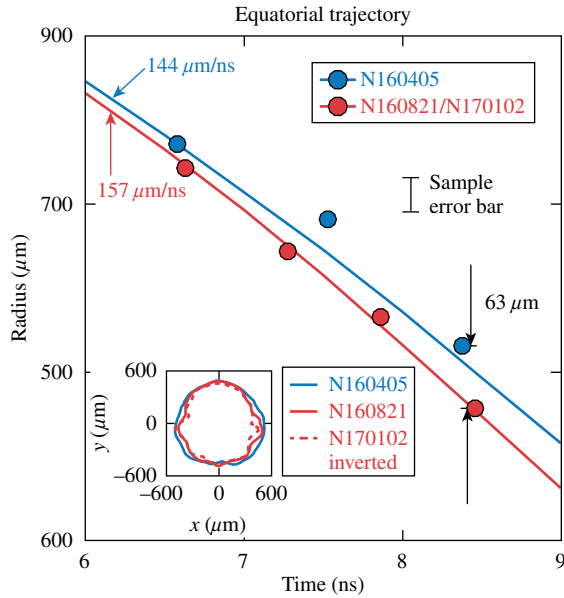


FIG. 5. Equatorial shell trajectories from postprocessed simulated (solid lines) and experimental (symbols) backlit radiographs. The red lines and symbols represent the baseline zero-detuning experiment (N160405). The blue lines and symbols represent the average of the two detuning experiments (N160821 and N170102). The inset shows superimposed extracted surfaces from the experimental radiographs of Fig. 4, exemplifying the equatorial mitigation.

result of wavelength-detuning CBET mitigation. The equatorial shell speed increases 9% from 144 to 157  $\mu\text{m}/\text{ns}$  based on simulation (experimentally a 16% increase from 133 to 154  $\mu\text{m}/\text{ns}$ ) because wavelength-detuning CBET mitigation deposits 3% additional energy within the small volume over the equator. The enhanced equatorial velocity is consistently observed when comparing the extracted outer shell contours taken from zero detuning and detuning shots in Fig. 5 (inset), where the entire surface-area-weighted average implosion speed increases experimentally by 13%.

In conclusion, the first direct-drive wavelength-detuning CBET mitigation experiments on the NIF with a modest wavelength difference between crossing beams confirmed improved coupling predicted by multidimensional hydrodynamic simulations. These direct-drive proof-of-principle experiments are the first such experiments and provide a path forward to recovering the energy loss caused by CBET. Simulations predict that, as the wavelength separation increases (e.g., the  $\pm 6\text{-\AA}$  UV predicted NIF limit), the equatorial drive continues to improve and requires rebalancing to minimize  $\ell = 2$ . Simulations also indicate that judicious use of all three colors with flexible color mapping in the fiber front end on the NIF produces better-balanced CBET mitigation designs in PDD. Simulations predict that symmetric direct drive on OMEGA will benefit from wavelength detuning since its three main driver legs

already distribute evenly over the target. Additional CBET mitigation domains may be combined with wavelength detuning, e.g., optimized spot shapes that reduce the laser energy refracting over the horizon while maintaining optimal shape [spot-masking apodization (SMA)] [18]. Future experiments are planned to scope out the capabilities of wavelength-detuning CBET mitigation to further improve coupling and to address the asymmetry by proposing system changes to both OMEGA and the NIF: adding multiple wavelength sources to OMEGA, expanding the NIF's wavelength-detuning range, using SMA-DPPs, different wavelengths within NIF's quads, and remapping the NIF fiber front end to obviate cone swapping.

This material is based upon work supported by the Department of Energy National Nuclear Security Administration under Award No. DE-NA0001944, the University of Rochester, and the New York State Energy Research and Development Authority. This report was prepared as an account of work sponsored by an agency of the U.S. Government. Neither the U.S. Government nor any agency thereof, nor any of their employees, makes any warranty, express or implied, or assumes any legal liability or responsibility for the accuracy, completeness, or usefulness of any information, apparatus, product, or process disclosed, or represents that its use would not infringe privately owned rights. Reference herein to any specific commercial product, process, or service by trade name, trademark, manufacturer, or otherwise does not necessarily constitute or imply its endorsement, recommendation, or favoring by the U.S. Government or any agency thereof. The views and opinions of authors expressed herein do not necessarily state or reflect those of the U.S. Government or any agency thereof.

\*Corresponding author.

jimijam@le.rochester.edu

- [1] M. C. Herrmann, M. Tabak, and J. D. Lindl, A generalized scaling law for the ignition energy of inertial confinement fusion capsules, *Nucl. Fusion* **41**, 99 (2001).
- [2] C. J. Randall, J. R. Albritton, and J. J. Thomson, Theory and simulation of stimulated brillouin scatter excited by non-absorbed light in laser fusion systems, *Phys. Fluids* **24**, 1474 (1981).
- [3] T. R. Boehly, D. L. Brown, R. S. Craxton, R. L. Keck, J. P. Knauer, J. H. Kelly, T. J. Kessler, S. A. Kumpan, S. J. Loucks, S. A. Letzring *et al.*, Initial performance results of the OMEGA laser system, *Opt. Commun.* **133**, 495 (1997).
- [4] E. M. Campbell and W. J. Hogan, The national ignition facility—Applications for inertial fusion energy and high-energy-density science, *Plasma Phys. Controlled Fusion* **41**, B39 (1999).
- [5] C. J. McKinstrie, J. S. Li, R. E. Giacone, and H. X. Vu, Two-dimensional analysis of the power transfer between crossed laser beams, *Phys. Plasmas* **3**, 2686 (1996).

- [6] C. J. McKinstrie, A. V. Kanaev, V. T. Tikhonchuk, R. E. Giacone, and H. X. Vu, Three-dimensional analysis of the power transfer between crossed laser beams, *Phys. Plasmas* **5**, 1142 (1998).
- [7] P. B. Radha, V. N. Goncharov, M. Hohenberger, T. C. Sangster, R. Betti, R. S. Craxton, D. H. Edgell, R. Epstein, D. H. Froula, J. A. Marozas *et al.*, Direct-drive implosion physics: Results from OMEGA and the national ignition facility, *J. Phys.: Conf. Ser.* **688**, 012006 (2016).
- [8] M. Hohenberger, P. B. Radha, J. F. Myatt, S. LePape, J. A. Marozas, F. J. Marshall, D. T. Michel, S. P. Regan, W. Seka, A. Shvydky *et al.*, Polar-direct-drive experiments on the national ignition facility, *Phys. Plasmas* **22**, 056308 (2015).
- [9] D. Cao, G. Moses, and J. Delettrez, Improved non-local electron thermal transport model for two-dimensional radiation hydrodynamics simulations, *Phys. Plasmas* **22**, 082308 (2015).
- [10] J. Delettrez, R. Epstein, M. C. Richardson, P. A. Jaanimagi, and B. L. Henke, Effect of laser illumination nonuniformity on the analysis of time-resolved X-ray measurements in uv spherical transport experiments, *Phys. Rev. A* **36**, 3926 (1987).
- [11] P. B. Radha, V. N. Goncharov, T. J. B. Collins, J. A. Delettrez, Y. Elbaz, V. Yu. Glebov, R. L. Keck, D. E. Keller, J. P. Knauer, J. A. Marozas *et al.*, Two-dimensional simulations of plastic-shell, direct-drive implosions on OMEGA, *Phys. Plasmas* **12**, 032702 (2005).
- [12] V. N. Goncharov, T. C. Sangster, R. Betti, T. R. Boehly, M. J. Bonino, T. J. B. Collins, R. S. Craxton, J. A. Delettrez, D. H. Edgell, R. Epstein *et al.*, Improving the hot-spot pressure and demonstrating ignition hydrodynamic equivalence in cryogenic deuterium—Tritium implosions on OMEGA, *Phys. Plasmas* **21**, 056315 (2014).
- [13] P. Michel, L. Divol, E. A. Williams, C. A. Thomas, D. A. Callahan, S. Weber, S. W. Haan, J. D. Salmonson, N. B. Meezan, O. L. Landen *et al.*, Energy transfer between laser beams crossing in ignition hohlraums, *Phys. Plasmas* **16**, 042702 (2009).
- [14] I. V. Igumenshchev, W. Seka, D. H. Edgell, D. T. Michel, D. H. Froula, V. N. Goncharov, R. S. Craxton, L. Divol, R. Epstein, R. Follett *et al.*, Crossed-beam energy transfer in direct-drive implosions, *Phys. Plasmas* **19**, 056314 (2012).
- [15] M. L. Spaeth, K. R. Manes, D. H. Kalantar, P. E. Miller, J. E. Heebner, E. S. Bliss, D. R. Speck, T. G. Parham, P. K. Whitman, P. J. Wegner *et al.*, Description of the NIF Laser, *Fusion Sci. Technol.* **69**, 25 (2016).
- [16] S. Skupsky, J. A. Marozas, R. S. Craxton, R. Betti, T. J. B. Collins, J. A. Delettrez, V. N. Goncharov, P. W. McKenty, P. B. Radha, T. R. Boehly *et al.*, Polar direct drive on the national ignition facility, *Phys. Plasmas* **11**, 2763 (2004).
- [17] J. A. Marozas, F. J. Marshall, R. S. Craxton, I. V. Igumenshchev, S. Skupsky, M. J. Bonino, T. J. B. Collins, R. Epstein, V. Yu. Glebov, D. Jacobs-Perkins *et al.*, Polar-direct-drive simulations and experiments, *Phys. Plasmas* **13**, 056311 (2006).
- [18] J. A. Marozas, T. J. B. Collins, J. D. Zuegel, P. W. McKenty, D. Cao, S. Fochs, and P. B. Radha, Continuous distributed phase-plate advances for high-energy laser systems, *J. Phys.: Conf. Ser.* **717**, 012107 (2016).
- [19] S. X. Hu, D. T. Michel, A. K. Davis, R. Betti, P. B. Radha, E. M. Campbell, D. H. Froula, and C. Stoeckl, Understanding the effects of laser imprint on plastic-target implosions on OMEGA, *Phys. Plasmas* **23**, 102701 (2016).
- [20] T. P. Gill, *The Doppler Effect: An Introduction to the Theory of the Effect* (Logos, London, 1965).
- [21] J. J. MacFarlane, I. E. Golovkin, P. Wang, P. R. Woodruff, and N. A. Pereyra, SPECT3D—A multi-dimensional collisional-radiative code for generating diagnostic signatures based on hydrodynamics and PIC simulation output, *High Energy Density Phys.* **3**, 181 (2007).